Tropical Ocean Decadal Variability and Resonance of Planetary Wave Basin Modes. Part I: Theory*

Z. LIU

Center for Climatic Research/IES, Madison, Wisconsin, and Department of Atmospheric and Oceanic Sciences, University of Wisconsin—Madison, Madison, Wisconsin

(Manuscript received 23 July 2002, in final form 4 November 2002)

ABSTRACT

Oceanic response to decadal wind forcing is studied in a tropical–extratropical basin using two classical theoretical shallow water wave models: the equatorial wave model and the planetary wave model. Extratropical winds are found to generate significant thermocline variability in the tropical ocean with a spectral peak at decadal timescale; the preferred decadal time of the response is due to the resonance of the gravest planetary wave basin modes. The resonant response, however, is unimportant in the interior extratropical ocean, where it is distorted by the forced response to local Ekman pumping. It is proposed that the resonance of planetary wave basin modes may provide a mechanism for the generation of decadal variability in the tropical ocean and, potentially, in the coupled ocean–atmosphere system.

1. Introduction

Significant decadal climate variability has been observed in the tropical Pacific (e.g., Zhang et al. 1997) and Atlantic (e.g., Hastenrath 1978; Houghton and Tourre 1992) Oceans. The origin of the tropical decadal climate variability, however, remains elusive. One fundamental difficulty is our poor understanding of the long-term memory of tropical ocean dynamics. Unifying the classical theories for the equatorial wave and the extratropical planetary wave, we (Liu 2002, hereafter LIU) found recently that the low-frequency tropical basin modes, or the scattering modes of Jin (2001), are identical to the planetary wave basin modes (hereafter PB modes) of Cessi and Louazel (2001). Furthermore, the period of the gravest tropical basin mode equals the cross-basin time of the planetary wave along the poleward boundary of the basin.

As a follow-up of LIU, here we use both the equatorial and midlatitude planetary wave theories to investigate the response of a tropical–extratropical basin to variable wind forcing. Special attention will be paid to the response in the tropical ocean. Cessi and Louazel (2001) have noticed that in the planetary wave model, a basinwide extratropical wind forces a resonant response of the gravest PB mode, with a decadal power spectral peak. Using the equatorial wave model, Wang (2001, ch. 5) also suggests that the off-equatorial wind can contribute to the decadal variability of the tropical ocean. Our contribution here is to show, with both the planetary wave model and the equatorial wave model, that the resonant response of the PB mode is dominant for the thermocline variability in the Tropics and along the eastern boundary, but not in the interior extratropical ocean. Instead, the extratropical interior thermocline variability is distorted significantly by the nonresonant response to local winds, as studied by Frankignoul et al. (1997). The paper is arranged as follows. The models and solutions are presented in section 2. Forced oceanic responses are studied in sections 3 and 4 for localized winds and in section 5 for basinwide winds. A summary and some discussions are given in section 6.

2. Models and solutions

In the shallow-water system, oceanic responses to a periodic, or stochastic, forcing have been studied theoretically in many previous works, but all separately using either the equatorial wave theory or the planetary wave theory. For completeness, these solutions will be briefly described here. After the long-wave approximation, the linearized shallow water system forced by an anomalous zonal wind stress τ^x can be written on the equatorial β plane as

$$\partial_t u - yv = -\partial_x h + \tau, \tag{2.1a}$$

$$yu = -\partial_y h, \tag{2.1b}$$

$$\partial_t h + \partial_x u + \partial_y v = 0. \tag{2.1c}$$

* Center for Climatic Research Contribution Number 809.

Corresponding author address: Z. Liu, 1225 W. Dayton St., Madison, WI 53706.
E-mail: zliu3@facstaff.wisc.edu

This system has been nondimensionalized by the equatorial deformation radius $L_D = (c_0/\beta)^{1/2}$ for y, the basin width L for x, the Kelvin wave crossing time L/c_0 for t, the mean depth D for h, the Kelvin wave speed c_0 and c_0L_D/L for u and $v(c_0 = \sqrt{g'D})$, and $L/(\rho D c_0^2)$ for τ^x. We will consider an ocean basin bounded within $0 < x < 1$ and $0 < y < Y_N$, and, for simplicity, we only study the hemispheric symmetric response. With typical parameters of $\beta = 2 \times 10^{-11}$ m s^{-1}, $D = 400$ m and $g' = 0.02$ m s^{-2}, L_D is about 377 km. For the Pacific basin of $L \sim 10\,000$ km, the dimensional time unit L/c_0 is about 40 days.

In this paper, we will use a zonally uniform and temporally periodic wind stress,

$$\tau = \tau_0(y)e^{i\omega t}. \tag{2.2}$$

We will mainly study the oceanic response as a function of forcing frequency. The fact that the forcing amplitude in (2.2) is independent of frequency assures that the amplitude response of the ocean at different frequencies can also be treated as the power spectrum response to a stochastic (temporally white) forcing.

a. Forced equatorial wave solution

Assuming a forced response in (2.1) of the form of $h_E = H_E(x, y)e^{i\omega t}$, we will expand the dependent variables on parabolic cylinder functions (Cane and Sarachik 1981; Battisti 1988; Wang 2001, chapter 5):

$$\psi_m(y) = (-1)^m(2^m m!\sqrt{\pi})^{-1/2}e^{y^2/2}\frac{d^m e^{-y^2}}{dy^m}.$$

Applying the eastern ($u|_{x=1} = 0$) and western ($\int_0^\infty u|_{x=0}dy = 0$) boundary conditions, we have the full equatorial wave solution:

$$H_E(x, y) = 0.5\left\{\sum_{n=0}^{N}[Q_{2n}(x) + R_{2n}(x)]\psi_{2n}(y)\right\}, \tag{2.3}$$

with $R_{2(n-1)} = Q_{2n}\sqrt{2n/(2n-1)}$. Here

$$Q_0(x) = \left[Q_0(0) + \int_0^x F_0(\xi)e^{i\omega\xi}\,d\xi\right]e^{-i\omega x} \quad \text{and}$$

$$Q_{2n}(x) = \left[Q_{2n}(1)e^{-i(4n-1)\omega} + \int_x^1 F_{2n}(\xi)e^{-i(4n-1)\omega\xi}\,d\xi\right]e^{i(4n-1)\omega x}$$

represent the contributions from the equatorial Kelvin wave and equatorial Rossby waves, respectively. The coefficients of the solution are

$$Q_0(0) = \frac{G_0\sum_{n=1}^{N}A_n + \sum_{n=1}^{N}B_nG_{2n}}{1 - \sum_{n=1}^{N}A_n},$$

$$Q_{2n}(1) = Q_0(1)\sqrt{\frac{(2n-1)!!}{(2n)!!}},$$

$$Q_0(1) = [Q_0(0) + G_0]e^{-i\omega},$$

$$A_n = \frac{(2n-3)!!}{(2n)!!}e^{-i4n\omega},$$

$$B_n = \sqrt{\frac{(2n-3)!!}{(2n)!!(2n-1)}},$$

where the forcing is projected as

$$G_0 = \int_0^1 F_0e^{i\omega x}\,dx, \qquad G_{2n} = \int_0^1 F_{2n}e^{-i(4n-1)\omega x}\,dx,$$

$$F_0 = \int_{-\infty}^{\infty}\tau_0(y)\psi_0(y)\,dy,$$

$$F_{2n} = \int_{-\infty}^{\infty}\tau_0(y)[(2n-1)\psi_{2n}(y) - \sqrt{(2n-1)(2n)}\psi_{2(n-1)}(y)]\,dy,$$

$$n = 1, 2, 3, \ldots,$$

and $(2n)!! = 2 \times 4 \times \cdots \times (2n-2) \times 2n$, $(2n-1)!! = 1 \times 3 \times \cdots \times (2n-3) \times (2n-1)$, $(-1)!! = 1$. Setting the denominator of Q_0 to zero, we have the eigenvalue equation

$$1 - \sum_{n=1}^{N}\frac{(2n-3)!!}{(2n)!!}e^{-4in\sigma} = 0, \tag{2.4}$$

which gives (complex) eigenvalues $\sigma = \sigma_r + i\sigma_i$ for the free modes (Jin 2001).

b. Forced planetary wave solution

The forced planetary wave response h_P can be derived following Cessi and Louazel (2001). Neglecting $\partial_t u$ in (2.1a), we have from (2.1) the planetary wave equation

$$\partial_t h_P - (1/y^2)\partial_x h_P = w_e, \tag{2.5}$$

where $1/y^2$ is the westward planetary wave speed along latitude y and

$$w_e = -\partial_y(\tau/y) \tag{2.6}$$

is the Ekman pumping. With the wind of (2.2), the Ekman pumping is $w_e = w_0(y)e^{i\omega t}$, where $w_0(y) = -\partial_y(\tau_0/y)$. Assuming the planetary wave solution of the form $h_P = H_P(x, y)e^{i\omega t}$, the full response solution that satisfies the eastern boundary condition $u|_{x=1} = 0$ is

$$H_P(x, y) = H_0 + H_F, \tag{2.7a}$$

where

$$H_0 = H_1e^{iy^2\omega(x-1)} \tag{2.7b}$$

is the contribution from the eastern boundary and

$$H_F = \frac{w_o(y)}{i\omega}[e^{iy^2\omega(x-1)} - 1] \tag{2.7c}$$

is the contribution from the local forcing. The eastern boundary response H_1 is determined by the mass conservation $\int_0^{Y_N}\int_0^1 H_P\, dx\, dy = 0$ as

$$H_1 = -\frac{\int_0^{Y_N} w_0(y)[1 - (1 - e^{-i\omega y^2})/(i\omega y^2)]\, dy}{\int_0^{Y_N}(1 - e^{-i\omega y^2})/y^2\, dy}. \tag{2.8}$$

The (complex) eigenvalues $\sigma = \sigma_r + i\sigma_i$ of the free basin modes, or PB modes, can be obtained from

$$\int_0^{Y_N}(1 - e^{-i\sigma y^2})/y^2\, dy = 0, \tag{2.9}$$

which is derived by setting to zero the denominator of H_1.

c. *Equivalence of planetary and equatorial wave solutions*

In the low-frequency limit, on an infinite beta plane, the classical equatorial wave solution (2.3) is valid strictly only with an infinite truncation $N \to \infty$. In a finite basin $[-Y_N, Y_N]$, LIU showed that the truncation N should be finite to assure the absence of mass flux across the poleward boundaries and in turn the mass conservation within the basin. Indeed, beyond the critical latitude of a parabolic cylinder function $\psi_M(y)$ of $Y_{MC} \sim O(\sqrt{2M+1})$, the amplitudes of all the lower-order parabolic cylinder functions $\psi_m(y)$ $(m \le M)$ virtually diminish. In other words, with a truncation to order M, there will be virtually no current across the latitude Y_{MC}, assuring the mass conservation within Y_{MC}. Specifically, LIU showed that, for a given northern boundary of latitude Y_N, the truncation number N should be

$$N = Y_N^2/4, \tag{2.10a}$$

or, more precisely,

$$N = [Y_N^2/4] + 1, \tag{2.10b}$$

where brackets represent the integer part. Now, the N slowest free equatorial wave modes (especially the first few modes) in (2.4) (Jin 2001) correspond to the slowest PB modes in (2.9) (Cessi and Louazel 2001). Therefore, all these low-frequency basin modes will be called the PB modes hereafter regardless how they are derived. All the PB modes are weakly damped and their frequencies can be approximated as $\omega_{Pn} = n\omega_P$, $n = \pm 1, \pm 2, \cdots, \pm N/2$, where

$$\omega_P = 2\pi/Y_N^2 \tag{2.11}$$

is the frequency of the first PB mode, corresponding to the cross-basin time of the planetary wave along the northern boundary Y_N. In this paper, without loss of generality, we choose $N = 44$, corresponding to $Y_N = 13.23$. With our typical parameters that are given after Eq. (2.1), the dimensional northern boundary is at about 50°N and the first PB mode has a period about 20 yr.

The structure of the PB modes have two distinct features, in comparison with the higher-frequency equatorial basin modes (Cane and Moore 1981). While the equatorial basin modes tend to be equatorially trapped and have node points along the equator, the PB modes tend to have their maximum toward the northwestern corner of the basin and have no node points along the equator.

The condition (2.10) is the equivalence condition of the low-frequency equatorial and planetary wave solutions. As discussed in LIU, (2.10) assures the same free PB modes in the equatorial and planetary wave solutions. In the sections that follow, we will further show that (2.10) also guarantees a similar forced response of the equatorial wave solution (2.3) and the planetary wave solution (2.7) at low-frequency decadal timescales. The equivalence of the two seemingly very different forms of mathematical solutions (2.3) and (2.7) is not completely surprising. Neither (2.3) nor (2.7) has short Rossby waves, because of the geostrophic approximation in the v equation (2.1b) (the so-called long-wave approximation for equatorial waves). The only wave component that exists in the equatorial wave solution (2.3) but not in the planetary wave solution (2.7) is the equatorial Kelvin wave. For low-frequency basin adjustment, the role of the equatorial Kelvin wave is included implicitly in the planetary wave solution (2.7) with the condition of mass conservation, because the only function of the equatorial Kelvin wave is to transfer mass from the western to the eastern boundaries along the equator with effectively a negligible time delay (Liu et al. 1999).

3. Response to localized winds

The response of the equatorial ocean differs dramatically between an equatorial and an off-equatorial wind forcing. We first examine the oceanic response to a localized Gaussian wind profile:

$$\tau_0(y) = e^{-[(y-y_C)/l_y]^2}, \tag{3.1}$$

where $l_y = 0.1Y_N$ and y_C is the center latitude. With an equatorial wind ($y_C = 0$, Fig. 1b), the power spectrum of the equatorial thermocline at the eastern boundary exhibits a strong resonant peak at the frequency

$$\omega_{EB} = N\omega_P = \pi/2, \tag{3.2}$$

where we have used (2.10) and (2.11). This is seen in the equatorial wave solution H_E in Fig. 1a. The frequency (3.2) corresponds to a period of 4 times the cross-basin time of the equatorial Kelvin wave. This is because the gravest equatorial basin mode is established

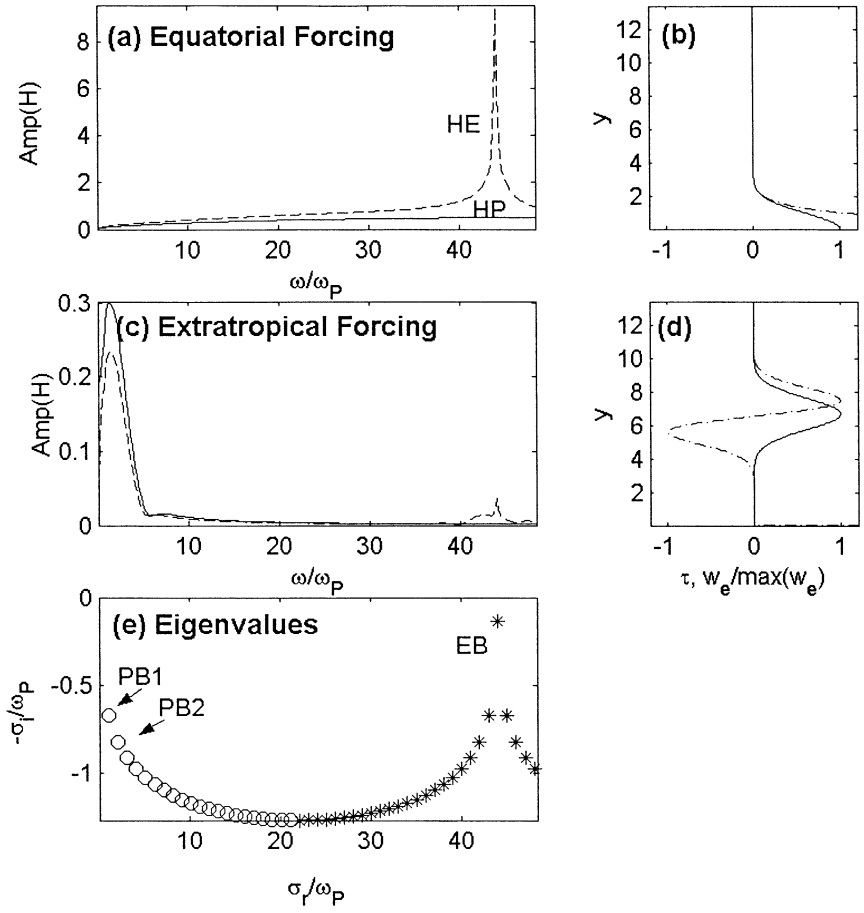

FIG. 1. Power spectra at the equatorial eastern boundary forced by the white noise wind of the Gaussian profile (3.1): (a) the spectra of the planetary wave solution H_P (solid) and equatorial wave solution H_E (dash) under (b) the wind patch centered on the equator (solid); (c) the spectra of H_P (solid) and H_E (dash) under (d) the wind patch centered at $y = 0.5Y_N$ (solid). The corresponding Ekman pumping velocity (normalized by its maximum magnitude) for each wind profile is also plotted (dash) in (b) and (d). (e) The damping rate $-\sigma_i$ and frequency σ_r of the eigenvalues of the free equatorial wave solution (2.4). The circles represent the PB modes, which have no node point on the equator, while the asterisks represent equatorial basin modes with one node point on the equator. All the frequencies and damping rates are normalized by the frequency of the first PB mode ω_P. The first two PB modes and the EB mode are also marked in (e).

after the eastward propagation of the equatorial Kelvin wave at the speed of $c_0 = \sqrt{g'D}$ and the westward propagation of the reflected first mode of equatorial Rossby wave at the speed of $c_0/3$. This peak response represents the resonant response of the slightly leaky equatorial basin mode (EB mode hereafter) of Cane and Moore (1981). This mode is of seasonal timescales and may be of relevance to the interannual ENSO variability (Neelin and Jin 1993). As shown in the eigenvalues of the equatorial wave model (Fig. 1e), $\omega_{\rm EB}$ represents the least damped oscillating mode. The pattern of the resonant response of the equatorial wave solution H_E at $\omega_{\rm EB}$ is similar to that of the free mode, with a large amplitude near the equator and a node point in the middle of the equator (as in Cane and Moore 1981, not shown). In comparison, no resonant peak is generated in the planetary wave solution H_P at $\omega_{\rm EB}$. Nevertheless, H_P simulates well the response of H_E in the lower-frequency range of the PB modes. This is because the PB modes are similar in the equatorial and planetary wave models only for modes that have frequencies no higher than about $(N/2)|\omega_P|$.

For an extratropical wind forcing ($y_C = 0.5Y_N$; Fig. 1d), in contrast, the dominant resonance peak occurs at the frequency of the first PB mode ω_P, while the resonance of the EB mode is very weak, as seen from H_E in Fig. 1c. Again, H_P is very similar to H_E only at the low-frequency range of the PB modes. The important message is that the extratropical wind could generate substantial equatorial decadal variability due to the resonant response of the PB modes, while the equatorial wind is more effective at higher frequencies to generate EB modes.

We now examine the evolution of forced response to

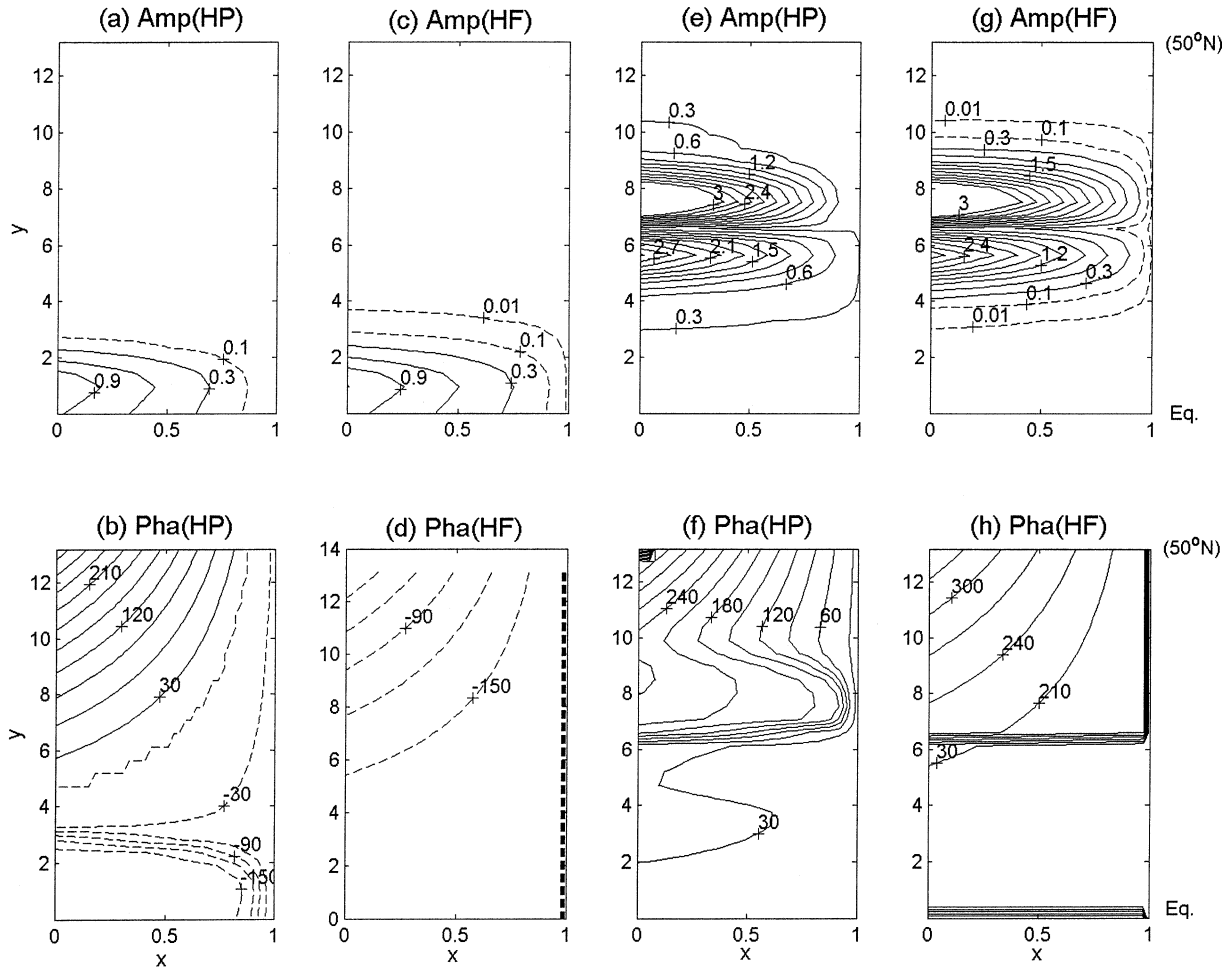

FIG. 2. Amplitude and phase of the forced response in the planetary wave solution (2.7) with the forcing frequency of ω_P: (a) amplitude and (b) phase of the full solution H_P (2.7a) forced by the equatorial wind in Fig. 1b; (c), (d) as in (a) and (b) but for the locally forced solution H_F in (2.7c). (e), (f) The full solution H_P as in (a) and (b) but under the extratropical wind of Fig. 1d; (g), (h) as in (e) and (f) but for the locally forced solution H_F. Contour intervals are 0.3 for the amplitude and 30° for the phase (negative phase in dash). Amplitudes larger than 3 are not plotted. Contour intervals of 0.1 and 0.001 are also plotted as dashed lines. The phase has been multiplied by -1 such that the wave propagates in the direction of increasing phase. Similar responses are found in the equatorial wave solution (2.3) (not shown). The dimensional y that is based on the typical parameters below (2.1) is also labeled at extreme right.

a decadal wind forcing of frequency ω_P. With the extratropical periodic wind (Fig. 1d), the dominant response is a dipole located in the region directly under the Ekman pumping forcing (about $4 < y < 9$) (Figs. 2e,f). The dipole consists of a southern pole and a northern pole separated by the zero Ekman pumping at about $y = 7$, and the amplitude of each pole largely increases westward. Outside the region of direct Ekman pumping, the response has a modest amplitude that is about the same as the eastern boundary. The phase evolution outside the forcing region follows the slow westward propagation of planetary waves at higher latitudes ($y > 9$) but is almost in phase with the eastern boundary at lower latitudes ($y < 4$) because of the faster propagation of planetary waves there. Along the northern boundary, the phase evolves with one complete cycle (360°) of the first PB mode, which is also one forcing period here.

The low-frequency response discussed above can be understood approximately from the Sverdrup balance. A planetary wave crosses the basin on the northern boundary Y_N in one forcing period $2\pi/\omega_P$. In the rest of the basin (which is located south of Y_N), planetary waves are faster and therefore would have crossed the basin by this time. This leaves behind an approximate Sverdrup balance

$$-(1/y^2)\partial_x h = -w_e, \tag{3.3a}$$

or after integration from the eastern boundary as

$$h = h_1 + h_F, \tag{3.3b}$$

where the full response h is the sum of the eastern boundary induced response $h_1 = h|_{x=1}$ and the locally forced response $h_F = (x - 1)y^2 w_e$. [Equations (3.3a) and (3.3b) can also be derived directly from (2.5) and

(2.7) at the low-frequency limit.] According to (3.3a,b), in the region directly forced by the local Ekman pumping dipole (dash in Fig. 1d), the amplitude of the response increases westward. Outside this direct forcing region, oceanic variability is caused completely by that on the eastern boundary.

Thermocline variability on the eastern boundary is important for the basin-mode response outside the forcing region but is not important in the forcing region. These can be seen in the locally forced solution H_F of (2.7c), which has no variability on the eastern boundary. Like in the full solution H (Fig. 2e), the amplitude of H_F (Fig. 2g) remains almost unchanged in the forcing region ($4 < y < 9$) and diminishes outside. The small effect of the eastern boundary thermocline on the response of the forcing region is due to the usually much weaker eastern boundary variability than that locally forced by the Ekman pumping (see the appendix).

The response along the eastern boundary H_0, and in turn in the Tropics, is almost in phase with the locally forced response H_F of the southern pole, but opposite to that of the (central and western part of the) northern pole (Fig. 2f). This occurs because mass conservation requires the eastern boundary thermocline to vary opposite to the net mass of H_F, which is contributed predominantly by the northern pole response (see the appendix for more discussion). A direct consequence of this eastern boundary phasing is a reinforcement of H_0 and H_F in the southern pole but a cancellation in the northern pole (in the eastern basin). Therefore, in spite of a stronger locally forced response H_F in the northern pole than in the southern pole (Fig. 2g), the full solution has a response stronger in the southern pole than in the northern pole (Fig. 2e) in the eastern part of the basin.

In the case of an equatorial wind (Fig. 1b), no resonant spectrum peak occurs on decadal timescales along the equator, as seen in Fig. 1a. The equator is now under direct wind forcing. The equatorial response shows a westward intensification (Fig. 2a) and an almost uniform phase (Fig. 2b), both reminiscent of the response of the northern pole under the extratropical forcing (Figs. 2e,f). Outside the equatorial forcing region, the amplitude of the response is about the same as that on the eastern boundary (about 0.07 in Fig. 2a); the phase follows the westward planetary wave radiating from the eastern boundary, again spanning one complete cycle at the northern boundary (Fig. 2b). As in the case of the extratropical forcing, in the region of Ekman pumping ($y < 3$), the locally forced response is dominant, while outside the forcing region the eastern boundary influence is necessary (Figs. 2c,d).

4. Resonance of planetary wave basin modes

To better understand the resonance of the PB modes, we examine the forced response to a set of Gaussian wind (3.1) that has the central latitude y_C shifting from the equator toward the northern boundary. The power spectra of the planetary wave solution H_P for different wind forcings are plotted on the equator and a subtropical latitude in Figs. 3a–d and Figs. 3e–h, respectively.

On the equator, for a given forcing frequency, the amplitude of the eastern boundary response tends to reach a maximum for an off-equatorial wind, with the central latitude of the maximum forcing increasing from $y_C \approx 3$ at higher frequency ($\approx 5\omega_P$) to $y_C \approx 6$ at the low-frequency limit (Fig. 3a). Similar maximum response to the off-equatorial wind can be found in the midbasin (Fig. 3b) and in the zonal-mean response (Fig. 3c) on the equator. This is consistent with Wang (2001, ch. 5), who has found that, for certain decadal forcing, the equatorial response is maximum to an off-equatorial wind centered around 11° ($y_C \approx 3$ in our nondimensional y). Here, however, we should point out that this latitude of most effective wind forcing is valid only at frequencies higher than about $3\omega_P$. At lower frequencies, the maximum forcing has a much broader frequency range from $y_C \approx 3$ to 10 (Figs. 3a–c). Therefore, practically, all the extratropical forcings are effective in generating equatorial variability.

The most important result of this work is that the equatorial response to extratropical forcings has a dominant resonant peak (Figs. 3a–c). As y_C moves away from the equator to $y_C > 4$, the resonance frequency decreases toward the first mode (at ω_P) and the power spectral peak becomes more and more distinguished. This resonant response is rather uniform along the equator, as seen in the similar spectra at the eastern boundary (Fig. 3a), the midbasin (Fig. 3b), and of the zonal mean (Fig. 3c). This uniform resonant response to the extratropical wind is also seen in the almost zero phase difference between the responses at the eastern and western boundaries (Fig. 3d) and is consistent with the example in Figs. 2e,f.

Equatorial wind (say, $y_C < 1$), although inefficient in generating variability on the eastern boundary (Fig. 3a), can generate substantial variability away from the eastern boundary, as shown by a secondary maximum response in the midbasin (Fig. 3b) and in the zonal mean (Fig. 3c; for $y_C = 0$). Different from the extratropical wind, however, the equatorial wind does not generate resonant equatorial peak responses at the decadal PB-mode frequencies (Figs. 3a–c); instead, it generates a power spectrum that increases toward higher frequencies (and resonates toward the EB mode, as shown in Fig. 1a). The interior equatorial ocean has a response that is larger than that on the eastern boundary because of a nonuniform zonal response to the equatorial wind. Indeed, the east–west phase difference increases (from about zero at $y_C > 2$) to about 120° when $y_C \approx 0$ (Fig. 3d), indicating an apparent eastward propagation. It should, however, be noticed that this eastward propagation occurs only near the eastern boundary in a narrow region, as seen in the sharp phase change there in the example of Fig. 2b. As a result, the equatorial ocean remains largely in phase with the amplitude increasing toward the west. This can be seen in the example of

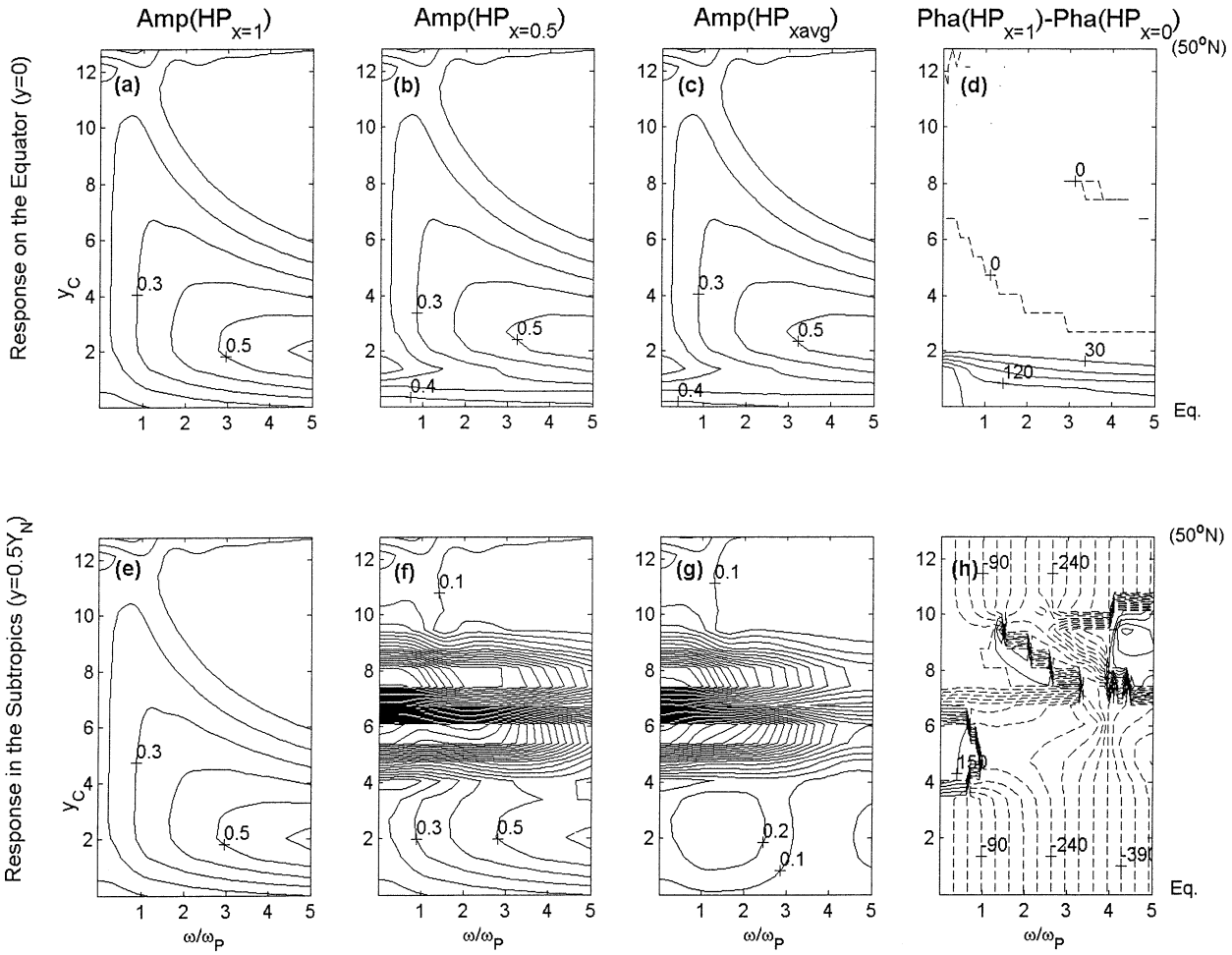

FIG. 3. Low-frequency power spectra of the planetary wave model solution H_P in (2.7) for Gaussian wind (3.1) centered at different latitudes y_C. (a),(b),(c) The equatorial power spectra at the eastern boundary ($x = 1$), midbasin ($x = 0.5$), and for the zonal mean, respectively; (d) the phase difference between the eastern ($x = 1$), and western ($x = 0$) boundaries (positive means eastward propagation). (e)–(h) As in (a)–(d) but for the responses in the subtropics at $y = 0.5Y_N$. The contour intervals are 0.1 for the amplitude and 30° for the phase difference. Before the calculation of the phase difference, a continuous phase is obtained at each point by an adjustment of the phase discontinuity that appeared in Fig. 2.

Figs. 2a,b. The in-phase change on the equator (away from the eastern boundary) results in a similar response of the zonal mean (Fig. 3c) and at the midbasin (Fig. 3b).

The equatorial wave solution H_E (Figs. 4a–d) shows a similar equatorial response to the planetary wave solution H_P discussed above (Figs. 3a–d). The planetary wave solution H_P is expected to simulate the equatorial response at decadal timescales. Indeed, given a forcing frequency, the planetary wave solution (2.7) has the limit $H_P(x, y) = H_0 + \tau^x(0)(x - 1)$ toward the equator, where we have used $w_0(y) = -\partial_y(\tau_0/y)$. Therefore, the equatorial wind is always balanced by the pressure gradient as in the Sverdrup balance (A.1). In other words, for the low-frequency PB modes, the adjustment of the equatorial Kelvin wave is infinitely fast and its role is negligible. Indeed, at such low frequencies, the equatorial Kelvin wave contributes little to the mass redistribution and then mass conservation of the basin modes (Liu et al. 1999).

In contrast to the tropical ocean, which is dominated by the resonant response of the lowest PB modes to extratropical winds, the extratropical region is affected little by the resonant PB modes, as shown in Figs. 3e–h on a subtropical latitude of $y = 0.5Y_N$. Along the eastern boundary, the subtropical response (Fig. 3e) is the same as on the equator (Fig. 3a) because of the constant h along the eastern boundary. In the interior ocean (Fig. 3f) (and in turn the zonal mean; Fig. 3g), however, the response differs dramatically from that on the eastern boundary. Most important is the lack of a resonant peak of the PB modes in Figs. 3f,g. In the latitudes directly under the wind forcing (roughly $4 < y_C < 9$), the midbasin and zonal mean responses are dominated by a red spectrum. This response is forced mainly by the local Ekman pumping on the same lati-

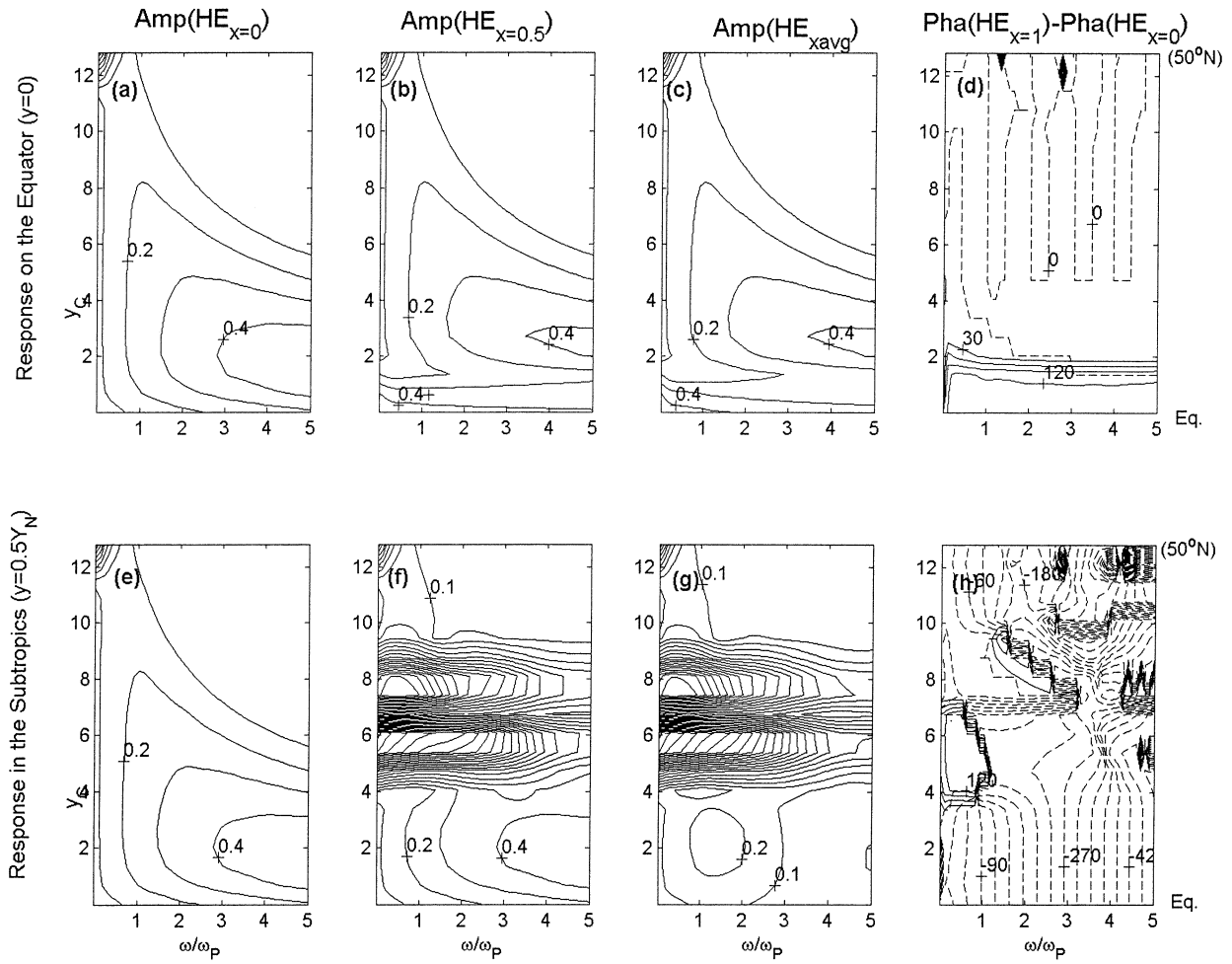

FIG. 4. As in Fig. 3 but for the equatorial wave model solution H_E in (2.3).

tude, as discussed by Frankignoul et al. (1997), and is affected little by the resonance of the PB modes. This difference of the interior and eastern boundary response has been noticed by Cessi and Louazel (2001). Indeed, this red spectrum response remains almost the same for the locally forced response H_F (not shown). The results here are consistent with the example in Figs. 2e–h, which show little influence of the eastern boundary on the locally forced response. The east–west phase difference shows a distorted structure (Fig. 3h) because of the superposition of free wave and locally forced responses, as seen in the example of Fig. 2f. Forced by wind patches on the equatorial side, the subtropical interior ocean has a power spectrum that increases toward higher frequencies (Fig. 3f), and the negative east–west phase difference (Fig. 3h) indicates a westward propagation of the planetary wave, as discussed in the example in Fig. 2f. It is nevertheless interesting to see a broad and weak resonant peak in the zonal mean response near the frequencies of the first and second PB modes, when forced by winds on the equatorial side ($2 < y_C < 4$) (Fig. 3g). Overall, the east–west phase difference is negative (Fig. 3f) due to the westward propagation of planetary waves. As in the case of the equatorial response (Figs. 3a–c and Figs. 4a–c), the subtropical responses are similar between the equatorial wave solution H_E (Figs. 4e–h) and the planetary wave solution H_P (Figs. 3e–h).

In short, with localized wind forcing, the tropical ocean is dominated by the resonant response of the PB modes to extratropical forcing, while the extratropical response is dominated by the locally forced response to Ekman pumping forcing. With an equatorial wind, the tropical response no longer exhibits resonant peak response of the PB modes but resonates with the EB modes at much higher frequencies. It is conceivable that, with a basin-scale wind, the response of the tropical ocean could be complicated by the competition of the equatorial and off-equatorial winds. This will be discussed below.

5. Response to basin-scale wind

Figure 5 shows the power spectra of the eastern boundary equatorial response under four different wind

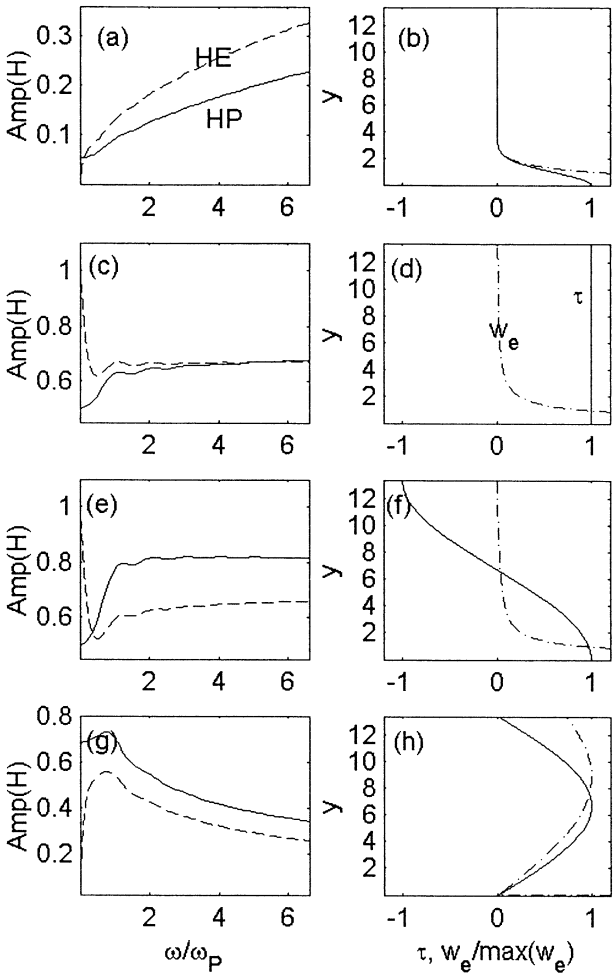

FIG. 5. (a),(c),(e),(g) Low-frequency power spectra at the equatorial eastern boundary forced by (b) a localized equatorial Gaussian wind; (d) a uniform wind; (f) a half cosine wind $\tau_0 = \cos(\pi y/Y_N)$; and (h) a half sine wind $\tau_0 = \sin(\pi y/Y_N)$, respectively. For the power spectra, the planetary wave solution H_P and equatorial wave solution H_E are plotted in solid and dash, respectively. For each wind profile (solid), the corresponding Ekman pumping is also plotted (dash) after normalized by its maximum magnitude.

forcings. With a localized equatorial wind (Fig. 5b, the same as Fig. 1b), no resonance peak occurs for the PB modes (Fig. 5a). As seen previously in Fig. 1a, this localized equatorial wind favors resonant EB-modes at higher frequencies. With a uniform wind (Fig. 5d), the power spectrum shows almost a white spectrum for the first few PB modes (Fig. 5c), with weak resonance peaks discernable for the first and second PB modes.[1] This is different from Cessi and Louazel (2001), who studied the response to the same uniform wind but in an off-equatorial basin. In their case, a distinctive resonant peak occurs for the first PB mode on the eastern boundary (their Fig. 5a). The much suppressed resonance peak in our case is due to the inclusion of the equator into the basin and the presence of the equatorial wind: the former increases the damping rate of the free PB mode[2] and the latter favors resonance of the higher-frequency EB mode, instead of the PB modes.

Similar to the uniform wind, with a half cosine wind profile in which the equatorial and midlatitude winds are of comparable magnitude but opposite signs (Fig. 5f), no clear resonance of PB modes occurs (Fig. 5). In contrast, with a half sine wind profile (Fig. 5h) in which the wind vanishes toward the equator, clear resonance peak response occurs for the first PB mode (Fig. 5g) as for the localized extratropical winds (Fig. 1c).

The spatial evolution of the forced response is also complicated by the simultaneous presence of extratropical and equatorial winds. For a basinwide extratropical wind such as the half sine wind in Fig. 5h, resonance occurs at the forcing frequency ω_P, with the maximum response in the northwest corner (Fig. 6a). The phase diagram shows a basinwide westward propagation (Fig. 6b), reminiscent of the propagation of planetary waves. The pattern of the amplitude resembles that of the first free PB mode (see Fig. 2 of LIU), with one important difference: the decrease of the amplitude from the northern boundary toward the equator is much smaller in the forced response than in the free mode. This difference is caused by the damped nature of the free PB modes. In the interior ocean toward the western boundary $x = 0$, the forced response may be approximated from (2.7) as $H_P \approx w_0 e^{i\omega_P y^2}$, while the free mode has the form $H_{P\text{free}} = e^{\sigma_1 y^2} \times e^{i\omega_P y^2}$, where $\sigma_1 > 0$ is the damping rate of the first PB mode. The ratio of the equatorial response to the northern boundary response is therefore $1/w_0 e^{i\omega_P Y_N^2}$ and $(1/e^{\sigma_1 Y_N^2}) e^{i\omega_P Y_N^2}$ for H_P and $H_{P\text{free}}$, respectively. The latter has a much reduced amplitude toward the equator because of the exponential factor $e^{\sigma_1 Y_N^2}$ [assuming $w_0(y)$ is relatively uniform]. Noticing $\sigma_1 \approx 0.65\omega_P$ (Cessi and Louazel 2001; LIU) and (2.11) this factor can be estimated as $e^{0.65\omega_P Y_N^2} \approx e^{0.65\times 2\pi} \approx 55$. Therefore, relative to the free PB mode, the equatorial response is much more significant in the forced resonant response.

In comparison, with a half cosine wind (Fig. 5f), which includes the competition of the equatorial and off-equatorial winds, the evolution of the response is completely different from the free mode. Now the amplitude shows little signature of any free PB mode (Fig. 6c), consistent with the lack of PB-mode resonance (Fig. 5e). It is interesting to see an eastward propagation in a broad tropical region, similar to those found in coupled GCM simulations (Liu et al. 2002). This eastward propagation is unrelated to the equatorial Kelvin wave, which has been filtered out in our planetary wave model: Instead, it is due to the interference between the locally forced response and the eastern boundary induced free

[1] With explicit mixing, the spectral peak is likely to favor the large-scale gravest PB mode.

[2] Roughly speaking, the damping rate of the PB modes increases with the difference of the maximum and minimum planetary wave speeds (or latitudes) in the basin (not shown).

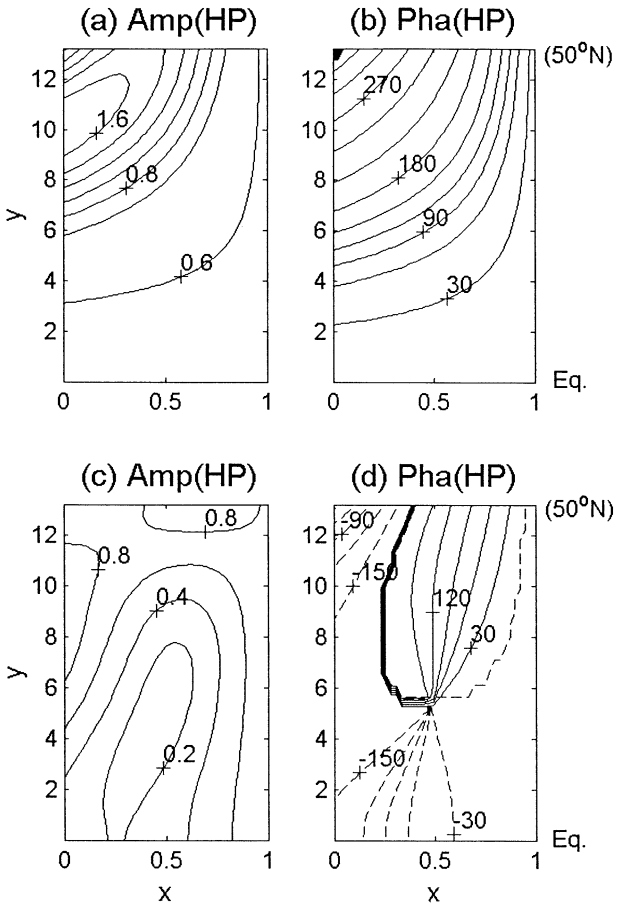

FIG. 6. Similar to Fig. 2, the spatial distribution of the (a) amplitude and (b) phase of the planetary wave solution H_P forced by the basin-wide half sine wind in Fig. 5h of frequency ω_P. (c),(d) As in (a) and (b), respectively, but under the half cosine forcing in Fig. 5f. Contour intervals are 0.2 for the amplitude and 30° for the phase. The phase is multiplied by -1 such that the signal propagates in the direction of increasing phase. The results are similar in the equatorial wave solution H_E (not shown).

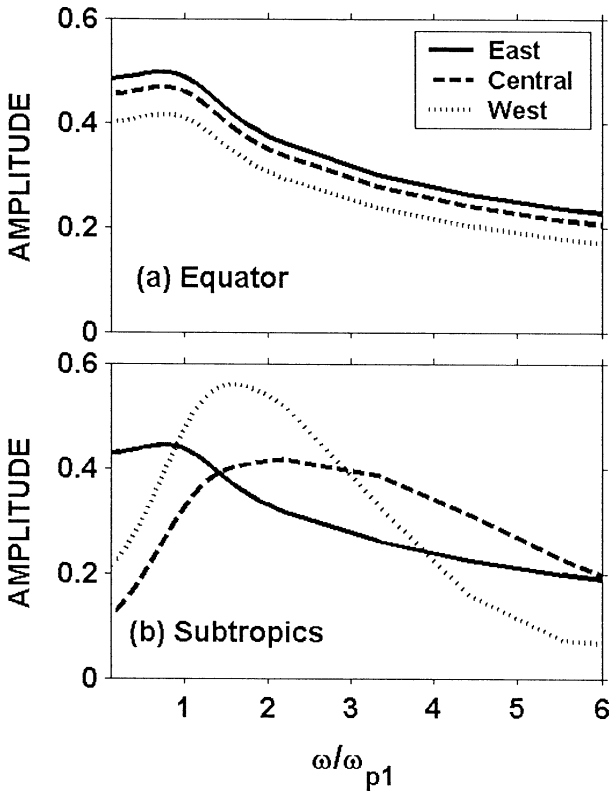

FIG. 7. A numerical solution of the full linear shallow water system [Eqs. (2.1) with an additional very small linear momentum damping, but without the long-wave approximation in (2.1b)]. The model is solved using the finite difference scheme of C grid. The equations are nondimensionalized similar to that in (2.1). The forcing has the form of (2.2) with $\tau_0(y)$ being a sine wind profile as in Fig. 5h. The basin dimension is similar to our standard case with a nondimensional domain of $0 \le x \le 1$, and $0 \le y \le 14$, with 18 and 30 grid points in the x and y directions. Power spectra of the oceanic variability are shown along (a) the equator ($y = 0$) and (b) subtropics ($y = 7$) near the eastern boundary ($x = 1$, solid), midbasin ($x = 0.5$, dash), and western boundary ($x = 0$, dot).

wave propagation. A similar eastward propagation can also be seen in the case of the localized equatorial forcing (Fig. 2b), where the eastward transition occurs rapidly in a narrow zone near the eastern boundary.

6. Summary and discussion

In this paper, we studied the oceanic response to external wind forcing in a tropical–extratropical basin with the focus on the tropical response to decadal forcing. Two classical theoretical wave models are used: the equatorial wave model and the planetary wave model. Both models produce the same result at decadal frequencies: under an extratropical wind forcing, the oceanic response in the Tropics, and the eastern boundary, is dominated by a resonant spectrum peak of the gravest PB modes. This resonant PB-mode response, however, is unimportant in the interior extratropical ocean, because of the overwhelming effect by local Ekman pumping. In contrast to the extratropical wind, an equatorial wind tends to generate resonance at much higher frequencies of the EB mode. The competition of the extratropical and equatorial wind may result in complex responses in the Tropics.

Our theoretical results are confirmed numerically in the full linear shallow water system that is solved using a finite-difference scheme (Yang and Liu 2002, manuscript submitted to *J. Phys. Oceanogr.*). Figure 7 shows one example of the power spectra of the oceanic variability from a numerical solution of the shallow water system forced by the sine wind profile shown in Fig. 5h. On the equator, oceanic responses are dominated by a resonance peak at the frequency of the first PB mode in the eastern boundary, midbasin, and western boundary (Fig. 7a). The shape of the power spectra of the equatorial response resembles closely to that of the planetary wave solution in Fig. 5g, although the amplitude

of the numerical solution is somewhat weaker.[3] In the subtropics (Fig. 7b), the eastern boundary response (solid) is characterized by the same spectral peak as that on the equator, while the interior responses (in the midbasin and western boundary) no longer have a fixed frequency of resonant peak. These subtropical responses are also consistent with the theoretical solutions.

Our conclusions here can be applied to a general basin, although we have limited our discussions to those symmetric about the equator. In a more general tropical–extratropical basin that is not asymmetric about the equator, the northern boundary and the southern boundary can be of different distances from the equator. Now, the slowest free PB mode is determined primarily by the cross-basin time of the planetary wave along the boundary that is farther away from the equator (not shown). For the forced response here, the resonant peak in the Tropics would still occur at this gravest PB mode frequency.

Our mechanism of resonant PB modes provides a new paradigm for decadal oceanic variability in the Tropics, with the extratropical wind providing the forcing and the extratropical ocean providing the memory, or preferred timescale. There have been some recent studies on decadal variability, mostly focusing on the midlatitude. In the linear context, two groups of mechanisms have been proposed for the generation of resonant spectral peak response. In the first group, analogous to the delayed oscillator for ENSO variability (Suarez and Schopf 1988), the delayed negative feedback is important (e.g., Latif and Barnett 1994; Gu and Philander 1997; Czaja and Marshall 2000). In this case, the preferred timescale is determined mainly by the delay time. In the second group, spatial resonance occurs for temporally stochastic forcing that varies spatially periodically (with at least one full cycle) down the direction of the signal propagation. In the case of current advection (Saravanan and McWilliams 1998), the forcing needs to change sign down the direction of the current; in the case of planetary wave propagation (Jin 1997), the forcing needs to change sign westward across the basin. The peak time is now determined by the half wavelength of the forcing and the speed of the signal propagation [planetary wave speed for Jin (1997) and advective speed for Saravanan and McWilliams (1998)]. In the Tropics, the importance of the off-equatorial wind on the low-frequency tropical modes have been recognized (Jin 2001; Wang 2001, ch. 5). However, it has remained unclear if there is a preferred response timescale. Here, we find that the extratropical stochastic wind can generate a tropical response with a decadal spectral peak. The spectral peak is due to the resonance of PB modes, whose timescale is determined by the basin geometry only. Therefore, the preferred response time is robust and inherent to the basin-scale oceanic variability. The use of the zonally uniform forcing (2.2) in our shallow-water system, which has a westward wave propagation, excludes the mechanism of spatial resonance. Instead, our resonant mechanism relies on the extratropical wind on the PB mode, whose timescale is determined by the slow planetary wave propagation on the northern boundary and whose basinwide structure is established by the rapid communication of coastal and equatorial Kelvin waves within the basin. Unlike in Cessi and Louazel (2001), who have focused on the midlatitude response in the context of the resonant PB modes, we found that the resonant PB mode is of fundamental importance for the Tropics but not for the extratropics.

The resonance of the PB mode provides a potential mechanism for the generation of decadal variability in the tropical ocean. For example, the strong stochastic forcing in the midlatitude could excite a resonant PB mode and produce a dominant decadal variability in the tropical ocean. This decadal equatorial oceanic variability may further affect the atmosphere and finally generate decadal variability in the coupled ocean–atmosphere system. This resonance of the PB mode may also shed light on some previously proposed mechanism of tropical decadal climate variability. For example, the resonance of the PB mode may be relevant to the decadal variability generated in the intermediate coupled model of Kleeman et al. (1999), which has found that the coupled decadal variability is determined by the perturbation advection [as opposed to the mean advection as proposed by Gu and Philander (1997)]. Much work is needed for a better understanding of the role of the resonant PB modes for coupled climate variability. In particular, the response of the tropical ocean could be complicated, as studied in section 5, because the atmosphere responds to a tropical SST anomaly both locally and remotely, and therefore the tropical ocean response depends on the winds in the equatorial as well as extratropical regions.

Acknowledgments. Part of the work was carried out during the author's sabbatical leave at the University of Tokyo and the Ocean University of Qingdao. The author would like to thank Prof. T. Yamagata of the Tokyo University and Prof. Q. Liu of the Ocean University of Qingdao for their hospitality. The author would also like to thank Dr. Haijun Yang for providing the numerical example in Fig. 7 and two reviewers for helpful comments. This work is supported by NOAA, NASA, and DOE.

APPENDIX

Eastern Boundary Response to Local Extratropical Forcing

Under a local extratropical forcing (Figs. 2e,f), oceanic responses in the eastern boundary and the Tropics are almost in phase with that in the locally forced south-

[3] At zero frequency, the power of the equatorial wave solution in Fig. 5g diminishes. This feature is likely to be wrong because it differs from both the planetary wave solution and the numerical solution, both of which tend to have a finite power at the zero frequency.

ern pole, but opposite to that in the (central–western part of the) northern pole (Fig. 2f). This may seem counterintuitive because the locally forced response H_F (Fig. 2g) is stronger in the northern pole than in the southern pole.

The phase of the eastern boundary response can be understood as follows. With the low-frequency limit of the Sverdrup balance (3.3b), the mass conservation

$$0 = \int_0^{Y_N}\int_0^1 h_1\, dx\, dy + \int_0^{Y_N}\int_0^1 h_F\, dx\, dy$$

gives

$$h_1 Y_N = -\int_0^{Y_N}\int_0^1 h_F\, dx\, dy = \frac{1}{2}\int_0^{Y_N} y^2 w_e\, dy \equiv \frac{1}{2}\int_0^N (-y\partial_y\tau^x + \tau^x)\, dy, \tag{A.1}$$

where we have used $h_1 Y_N = \int_0^{Y_N}\int_0^1 h_1\, dx\, dy$. With a symmetric Gaussian wind patch (3.1) in the extratropics, the wind curl $[-y\partial_y\tau^x$ in (A.1)] generates a dipole, which is stronger in the northern pole because of the factor of y. The Ekman transport $[\tau^x$ in (A.1)] further enhances the wind curl in the northern pole but reduces the wind curl in the southern pole. (For example, an eastward wind jet produces a cyclonic curl and upwelling Ekman in the northern part, but opposite in the southern part. The westerly wind also forces an equatorward Ekman transport that diverges because of the reduced Coriolis parameter toward the equator. This divergence enhances the upwelling Ekman pumping in the north but cancels the downwelling Ekman pumping in the south.) As a result, the locally forced response h_F is always larger in the northern than in the southern pole (Fig. 2g). The stronger h_F in the northern pole dominates the net mass of the locally forced solution $\int_0^{Y_N}\int_0^1 h_F\, dx\, dy$. Since mass conservation requires the eastern boundary mass contribution to cancel the net mass of the forced solution, the eastern boundary response is always the opposite sign to that of the net mass, or the northern pole mass, of the locally forced solution h_F as shown in (A.1).

The amplitude of the eastern boundary response is also determined by the magnitude of the net mass of the locally forced response $\int_0^{Y_N}\int_0^1 h_F\, dx\, dy$ as shown in (A.1). Therefore, the amplitude of the eastern boundary variability is usually smaller than the local response in the extratropics for two reasons. First, a localized wind jet, as in (3.1), always produces a dipole of Ekman pumping that has opposite signs in the two poles. The net mass contribution of the locally forced response therefore is the small residual after the cancellation of the mass contribution of the two poles (e.g., Figs. 2e–h). Second, even for an Ekman pumping patch of the same sign, the eastern boundary response would still be small relative to the locally forced response, if the Ekman pumping is localized only in a small area (relative to the basin). This follows because the eastern boundary response is determined by the basin average of the locally forced response—a point that is discussed in the basin adjustment study of Liu et al. (1999).

REFERENCES

Battisti, D. S., 1988: The dynamics and thermodynamics of a warm event in a coupled atmosphere–ocean model. *J. Atmos. Sci.*, **45,** 2889–2919.

Cane, M., and D. Moore, 1981: A note on low-frequency equatorial basin modes. *J. Phys. Oceanogr.*, **11,** 1578–1584.

——, and E. Sarachik, 1981: The response of a linear baroclinic equatorial ocean to periodic forcing. *J. Mar. Res.*, **39,** 651–693.

Cessi, P., and S. Louazel, 2001: Decadal oceanic response to stochastic wind forcing. *J. Phys. Oceanogr.*, **31,** 3020–3029.

Czaja, A., and J. Marshall, 2000: On the interpretation of AGCMs response to prescribed time-varying SST anomalies. *Geophys. Res. Lett.*, **27,** 1927–1930.

Frankignoul, C., P. Muller, and E. Zorita, 1997: A simple model of the decadal response of the ocean to stochastic wind forcing. *J. Phys. Oceanogr.*, **27,** 1533–1546.

Gu, D., and S. G. H. Philander, 1997: Interdecadal climate fluctuations that depend on exchanges between the tropics and extratropics. *Science,* **275,** 805–807.

Hastenrath, S., 1978: On modes of tropical circulation and climate anomalies. *J. Atmos. Sci.*, **35,** 2222–2231.

Houghton, R. W., and Y. M. Tourre, 1992: Characteristics of low-frequency sea surface temperature fluctuations in the tropical Atlantic. *J. Climate,* **5,** 765–771.

Jin, F. F., 1997: A theory of interdecadal climate variability of the North Pacific ocean–atmosphere system. *J. Climate,* **10,** 1821–1835.

——, 2001: Low-frequency modes of tropical ocean dynamics. *J. Climate,* **14,** 3874–3881.

Kleeman, R., J. P. McCreary, and B. A. Klinger, 1999: A mechanism for generating ENSO decadal variability. *Geophys. Res. Lett.,* **26,** 1743–1746.

Latif, M., and T. P. Barnett, 1994: Causes of decadal climate variability over the North Pacific and North America. *Science,* **266,** 634–637.

Liu, Z., 2002: How long is the memory of tropical ocean dynamics? *J. Climate,* **15,** 3518–3522.

——, L. Wu, and E. Bayler, 1999: Rossby wave–coastal Kelvin wave interaction in the extratropics. Part I: Low-frequency adjustment in a closed basin. *J. Phys. Oceanogr.*, **29,** 2382–2404.

——, ——, R. Gallimore, and R. Jacobs, 2002: Search for the origins of Pacific decadal climate variability. *Geophys. Res. Lett.*, **29,** 1404, doi:10.1029/2001GL013735.

Neelin, J. D., and F. F. Jin, 1993: Modes of interannual tropical ocean–atmosphere interaction—A unified view. Part II: Analytical results in the weak-coupling limit. *J. Atmos. Sci.*, **50,** 3504–3522.

Saravanan, R., and J. C. McWilliams, 1998: Advective ocean–atmosphere interaction: An analytical stochastic model with implications for decadal variability. *J. Climate,* **11,** 165–188.

Suarez, M. J., and P. S. Schopf, 1988: A delayed action oscillator for ENSO. *J. Atmos. Sci.*, **45,** 3283–3287.

Wang, X., 2001: Observational and analytical analysis of the Pacific decadal variability. Ph.D. thesis, University of Hawaii.

Zhang, Y., J. M. Wallace, and D. Battisiti, 1997: ENSO-like interdecadal variability: 1900–93. *J. Climate,* **10,** 1004–1020.